Control of Surface Area and Porosity of Co_3O_4 via Intercalation of Oxidative or Nonoxidative Anions in Hydrotalcite-like Precursors

Z. P. Xu and H. C. Zeng*

Department of Chemical and Environmental Engineering, Faculty of Engineering, National University of Singapore, 10 Kent Ridge Crescent, Singapore 119260

Received May 4, 2000. Revised Manuscript Received August 21, 2000

Monometal hydrotalcite-like compounds of $Co^{II}_{0.74}Co^{III}_{0.26}(OH)_{2.01}(NO_3)_{0.21}(CO_3)_{0.02}\cdot 0.6H_2O$ and $Co^{II}_{0.74}Co^{III}_{0.26}(OH)_{1.99}(CO_3)_{0.13}(NO_3)_{0.01}\cdot 0.7H_2O$ have been prepared via precipitation and anion-exchange methods. After being heated at 150−600 °C, the two precursor compounds were oxidatively converted to product spinel Co_3O_4. The chemical nature of the anions intercalated in the interlayer space of the compounds determines the ultimate crystallite size, surface area, and porosity of the oxide spinel. By selection of carbonate anions, Co_3O_4 with crystallite size of 7−34 nm and surface area of 17−150 m^2/g can be prepared at 150−600 °C. In particular, nanometer size Co_3O_4 crystallites (7−10 nm) has been synthesized at a temperature as low as 150−250 °C from the precursor compound $Co^{II}_{0.74}Co^{III}_{0.26}(OH)_{1.99}(CO_3)_{0.13}(NO_3)_{0.01}\cdot 0.7\ H_2O$. The roles of the different anions in the interlayer space are also discussed with respect to the thermal decomposition of the precursor compounds.

Introduction

Co_3O_4 spinel is an important transition metal oxide material that has been traditionally prepared by thermal decomposition of cobaltous salts at temperatures of 250−900 °C.[1] The precipitation technique is a common method used for Co_3O_4 preparation.[2−5] The cobaltous salts are first converted to metal hydroxides in basic solution. The precipitate products, such as brucite-like β-$Co(OH)_2$, are then thermally decomposed into the Co_3O_4 phase under normal atmospheric conditions, noting that 2/3 of the initial divalent cobalt have to be oxidized to the trivalent state during this conversion.[6,7]

In the β-$Co(OH)_2$ structure, a divalent cobalt cation is located in the center of the octahedron formed by six hydroxyl groups. The metal octahedra then share their edges to form two-dimensionally infinite sheets, which are similar to the basic structure of brucite $Mg(OH)_2$.[2] These brucite-like sheets can stack upon each other to build a three-dimensional network due to the presence of various chemical interactions between the sheets.[2] However, if some cobalt cations in the brucite-like sheets adopt the trivalent state, anions from the solution will then be intercalated into the intersheet space (interlayer space) to maintain charge neutrality for the solid,[2] which leads to the formation of hydrotalcite-like structure (named after the natural hydrotalcite compound, $Mg_6Al_2(OH)_{16}CO_3\cdot 4H_2O$, or $MgAlCO_3$-HT for short).[2,8]

We have recently synthesized a cobalt hydrotalcite-like compound, $Co^{II}Co^{III}NO_3$-HT, using an ambience-controlled method.[9] It has been found that the decomposition temperature of the cobalt hydroxides has been lowered from 222 °C in β-$Co(OH)_2$ to 185 °C in $Co^{II}Co^{III}$-NO_3-HT.[9] The staged oxidation performed during the synthesis in the latter case is apparently advantageous for the temperature lowering, as some of the cobalt cations have already been in the trivalent state.[9] One of the other causes that might be attributed to the temperature lowering is the spacer property of intercalated anions, because the anions physically separate the brucite-like sheets from each other and thus provide higher accessibility for oxygen to the solid matrix during the oxidative decomposition of the hydrotalcite-like compounds to Co_3O_4.

Furthermore, the chemical nature of an anion should not be ignored. For example, the fact that some anions are oxidative and some are not may affect the ultimate product Co_3O_4, because intercalated anions may act as an additional solid source of oxidant required in the Co_3O_4 formation. In this paper, we describe an investigation on the Co_3O_4 synthesis via intercalation of two different anions in the hydrotalcite-like compounds of $Co^{II}Co^{III}AO_3$-HT (A = N and C), where the molecular geometries of the two anions (NO_3^- and CO_3^{2-}) are chosen to be identical (D_{3h}). This allows us to focus only on differences in electronic property, redox reactivity, and number of the anions. Our results show that the chemical nature of the anions in the interlayer space determines the final surface-area and porosity properties of the Co_3O_4.

Experimental Section

Material Synthesis. The hydrotalcite-like compound intercalated with nitrate ions, $Co^{II}Co^{III}NO_3$-HT (Co−NO_3 for

* Corresponding author. Tel: +65 874 2896. Telefax: +65 779 1936. E-mail: chezhc@nus.edu.sg.

(1) Brauer, G. *Handbook of Preparative Inorganic Chemistry*; Academic Press: New York, 1965; p 1520.
(2) Cavani, F.; Trifiro, F.; Vaccari, A. *Catal. Today* **1991**, *11*, 173.
(3) Jacobs, J.-P.; Maltha, A.; Reintjes, J. G. H.; Drimal, J.; Ponec, V.; Brongersma, H. H. *J. Catal.* **1994**, *147*, 294.
(4) Markov, L.; Petrov, K.; Lyubchova, A. *Solid State Ionics* **1990**, *39*, 187.
(5) Markov, L.; Lyubchova, A. *J. Mater. Sci. Lett.* **1991**, *10*, 512.
(6) Oku, M.; Sata, Y. *Appl. Surf. Sci.* **1992**, *55*, 37.
(7) Pyatnitskii, L. V. *Analytic Chemistry of Cobalt*; Israel Program for Scientific Translations: Jerusalem, 1966; p 5.
(8) Reichle, W. T. *Solid State Ionics* **1986**, *22*, 135.
(9) (a) Xu, Z. P.; Zeng, H. C. *J. Mater. Chem.* **1998**, *8*, 2499. (b) Xu, Z. P.; Zeng, H. C. *Chem. Mater.* **1999**, *11*, 67.

10.1021/cm000371e CCC: $19.00
Published on Web 10/27/2000

short), was synthesized by quickly adding 20.0 cm^3 of 1.0 M $Co(NO_3)_2$ ($Co(NO_3)_2 \cdot 6H_2O$, >99.0%, Fluka) solution to 100.0 cm^3 of 0.5 M ammoniacal solution, which was prepurged with nitrogen gas at 40 cm^3 min^{-1} for 30 min to minimize dissolving CO_2 (from air). The above precipitation was then followed by an aging treatment with pure O_2 bubbling through the liquid (flow rate = 40 cm^3 min^{-1}) at 40 °C for 24 h. The precipitate was then collected by filtrating and fully washed with deionized water and finally dried in vacuo overnight. The hydrotalcite-like compound intercalated with carbonate anions, $Co^{II}Co^{III}CO_3$-HT ($Co-CO_3$ for short), was prepared by immersing 2.0 g of $Co-NO_3$ in 100.0 cm^3 of 0.05 M Na_2CO_3 solution for 4 h, followed by the similar postsynthesis treatment for the $Co-NO_3$.

To examine the surface-area and porosity changes with the calcination temperature, the as-prepared samples were calcined with static air in an electric furnace (Carbolite) at 150, 200, 250, 300, 400, 500, and 600 °C, respectively, for 2 h.

Materials Characterization. Structures of the compounds and their calcined samples were studied with X-ray diffraction (XRD) in a Shimadzu XRD-6000 X-ray diffractometer using Cu Kα radiation ($\lambda = 1.5418$ Å) in the range of $2\theta = 8-70°$. The intersheet spacing of the $Co-NO_3$ and $Co-CO_3$ compounds was determined from the diffraction peak positions with structural analysis software. The average crystallite sizes of the two samples as well as their calcined derivatives (i.e., cobalt oxides) were estimated using the Debye−Scherrer formula from the full-width-of-half-maximum (fwhm) of the most intense peaks.[10] To investigate the chemical bondings of the hydrotalcite-like compounds, Fourier transform infrared spectroscopy (FTIR, Bio-rad) spectra were recorded by diluting samples in KBr pellets.[9] Elemental analysis for nitrogen and carbon contents in the prepared compounds was carried out with a Perkin-Elmer 2400 CHN analyzer. The cobalt content in each hydrotalcite-like compound was measured by thermogravimetric analysis (TGA, Shimadzu TGA-50) based on decomposed product Co_3O_4 at 600 °C. The content of trivalent cobalt in each compound was determined by an iodometrical titration.[9]

The differential thermal analysis (DTA, Shimadzu DTA-50) and thermogravimetric analysis (TGA, Shimadzu TGA-50) were conducted in order to understand thermal behaviors of cobalt hydroxides. In each run, 15−20 mg of sample was heated at a rate of 10 °C min^{-1} in air or nitrogen flow at 40 cm^3 min^{-1}. To differentiate thermal processes at various heating stages, FTIR spectra were also recorded with the same KBr pellet technique for the $Co-NO_3$ and $Co-CO_3$ samples heated to a specified temperature in the DTA measurements.

In combined TGA−FTIR measurements (TGA 2050, TA Instruments/FTIR, Bio-Rad), gases evolved from the two hydrotalcite-like samples heated with TGA were introduced into a measurement cell by carrier gas air at a rate of 100 cm^3 min^{-1}, and then a series of FTIR spectra were recorded in about every 4 s. To monitor the infrared absorbance changes versus scanning time, i.e., versus temperature, the Gram−Schmidt reconstruction technique was used to construct the chromatogram from a collected set of interferograms.[11] This chromatogram is actually a measure of integrated absorbance in each IR spectrum versus time. For gaseous species H_2O, NO_2, and CO_2 that have their distinct IR vibrational modes, IR-based chromatograms can be created by integrating the absorbance over a specified wavenumber region of the actual absorbance spectra. In this work, the chromatograms of H_2O (1500−1200 cm^{-1}), NO_2 (2960−2800 cm^{-1}), and CO_2 (2400−2270 cm^{-1}) were thus created with respect to their characteristic IR absorptions. Since the three regions are not overlapped, the deduced chromatograms can be taken as dynamic measures of relative concentration of the evolved chemical species versus time or temperature upon the thermal decomposition of the two hydrotalcite-like compounds.

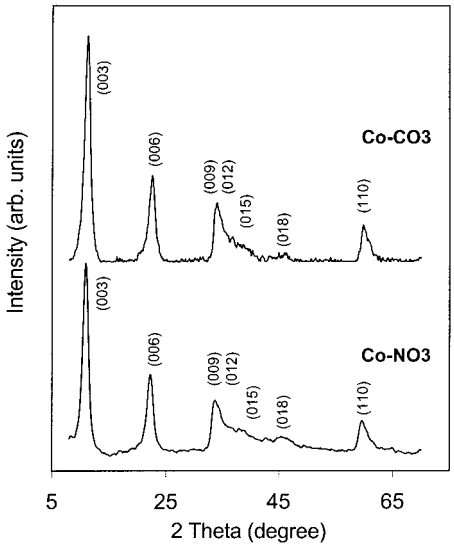

Figure 1. XRD patterns of two as-prepared hydrotalcite-like precursors, $Co-NO_3$ and $Co-CO_3$.

Table 1. Lattice Constants (Å) and Chemical Formulas for the Two As-Prepared Precursor Samples

sample	*a*	*c*	chem formula
$Co-NO_3$	3.08	23.9	$Co^{II}_{0.74}Co^{III}_{0.26}(OH)_{2.01}(NO_3)_{0.21}(CO_3)_{0.02} \cdot 0.6H_2O$
$Co-CO_3$	3.06	23.3	$Co^{II}_{0.74}Co^{III}_{0.26}(OH)_{1.99}(CO_3)_{0.13}(NO_3)_{0.01} \cdot 0.7H_2O$

Full adsorption−desorption isotherms of nitrogen at −195.8 °C on all calcined samples were measured at various partial pressures in a Quantachrome NOVA-1000 apparatus.[12] Specific surface areas (S_{BET}), pore volume, and pore-size distributions (PSD) were determined with the Brunauer−Emmett−Teller (BET)[13] method and Barret−Joyner−Hallenda (BJH)[14] method, respectively.

Results and Discussion

Chemical Compositions and Structures. The XRD patterns of Figure 1 indicate that the two prepared compounds have very similar hydrotalcite-like layered structures. According to the structural analysis (Table 1), lattice parameters (in rombohedral 3*R* symmetry) of $Co-NO_3$ are $a = 2d_{110} = 3.08$ Å and $c = 3d_{003} = 6d_{006} = 23.9$ Å, while those of $Co-CO_3$ are $a = 2d_{110} = 3.06$ Å and $c = 3d_{003} = 6d_{006} = 23.3$ Å. The similar *a* data indicate that the basic brucite-like sheet structure was not modified when the NO_3^- anions were replaced with CO_3^{2-} during the anion exchange (see Experimental Section). As expected, however, the interlayer spacing d_{003} (7.98 Å) of the $Co-NO_3$ is larger than those of $Co-CO_3$ (7.76 Å) and $Mg_6Al_2(OH)_{16}CO_3 \cdot 4H_2O$ (7.69 Å),[7,15] due to smaller affinity of monovalent anion NO_3^- compared to that of the divalent CO_3^{2-}.[2] On the basis of the fwhm analysis of XRD peaks, the crystallinities of both samples are very similar even though an additional anion exchange experiment was performed for the $Co-CO_3$.

(10) (a) Cheetham, A. K.; Day, P. *Solid-State Chemistry: Techniques*; Clarendon Press: Oxford, U.K., 1987; p 79. (b) Cullity, B. D. *Elements of X-ray Diffraction*; Addison-Wesley: Reading, MA, 1978; p 100.

(11) (a) Griffiths, P. R.; de Haseth, J. A. *Chemical AnalysisI*; Wiley-Interscience: New York, 1986; Vol. 83. (b) Akinade, K. A.; Campbell, R. M.; Compton, D. A. C. *J. Mater. Sci.* **1994**, *29*, 3802.

(12) (a) Chellam, U.; Xu, Z. P.; Zeng, H. C. *Chem. Mater.* **2000**, *12*, 650. (b) Ji, L.; Lin, J.; Zeng, H. C. *J. Phys. Chem. B* **2000**, *104*, 1783. (c) Ji, L.; Lin, J.; Zeng, H. C. *Chem. Mater.* **2000**, *12*, 931.

(13) Brunauer, S.; Emmett, P. H.; Teller, E. *J. Am. Chem. Soc.* **1938**, *60*, 309.

(14) Barrett, E. P.; Joyner, L. G.; Hallender, P. C. *J. Am. Chem. Soc.* **1951**, *73*, 373.

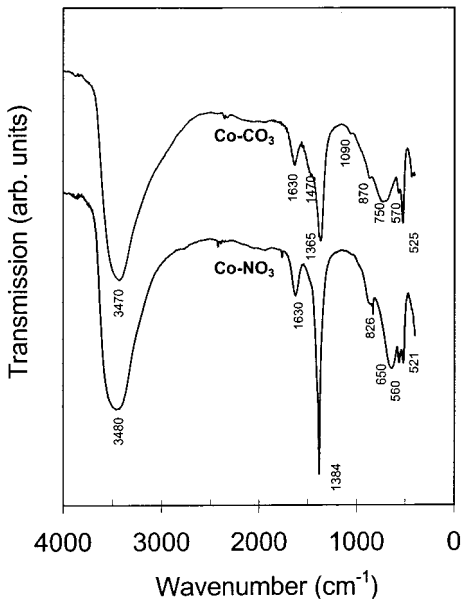

Figure 2. FTIR spectra of two as-prepared hydrotalcite-like precursors, $Co-NO_3$ and $Co-CO_3$.

The iodometrical titration indicates that about 26% of Co^{2+} was oxidized to Co^{3+} during the aging treatment. Our elemental analysis (CHN) and TGA study give the following two chemical formulas (Table 1) (i) $Co^{II}_{0.74}Co^{III}_{0.26}(OH)_{2.01}(NO_3)_{0.21}(CO_3)_{0.02}\cdot 0.6H_2O$ for the $Co-NO_3$ and (ii) $Co^{II}_{0.74}Co^{III}_{0.26}(OH)_{1.99}(CO_3)_{0.13}(NO_3)_{0.01}\cdot 0.7H_2O$ for the $Co-CO_3$, noting that the extra positive charge (Co^{3+}) in the brucite-like sheets and the negative charge (NO_3^- and CO_3^{2-} anions) in the interlayer space are balanced very well in the both compounds.

Figure 2 shows two FTIR spectra for above as-prepared samples. The broad bands around 3480 and 3470 cm^{-1} are attributed to the stretching vibration mode of OH groups (ν_{OH})[16−18] in the brucite-like sheets and the interlayer water molecules, noting that the δ_{HOH} mode of water is also observed at 1630 cm^{-1}.[16−18] An intense peak at 1385 cm^{-1} and a small peak at 826 cm^{-1} belong to the ν_3 and ν_2 vibrational modes of NO_3^-, respectively,[16,17,19] which reveals that the nitrate ions in the interlayer are lying parallel to the brucite-like sheets, preserving their D_{3h} symmetry. In addition to the ν_3 and ν_2 vibrational modes (1365 and 870 cm^{-1}, respectively)[6,20−22] observed, the $Co-CO_3$ spectrum shows two more absorptions at 1470 and 1090 cm^{-1} which belong to the ν_3 and ν_1 vibrational modes of carbonate anions with C_{2v} symmetry.[20−23] Apparently, the interlayer carbonate anions of $Co-CO_3$ are perturbed to acertain extent, as the symmetry lowering and an IR peak shift to 1365 cm^{-1} (versus 1415 cm^{-1} of free CO_3^{2-})[2,23] are observed. This perturbation can be attributed to stronger electrostatic interactions between the divalent CO_3^{2-} anions and the brucite-like sheets, compared to the relatively unperturbed (monovalent) nitrate anions in the $Co-NO_3$. The sharp peaks at 560 and 521 cm^{-1} in the $Co-NO_3$ should correspond to those at 570 and 525 cm^{-1} in the $Co-CO_3$; they can be assigned to Co−O vibrations.[6,24] Upon the anion exchange, the broad band at 650 cm^{-1} of the $Co-NO_3$ spectrum is shifted to 750 cm^{-1} in the $Co-CO_3$. The blue shift observed may be resulted from the weaker influence of CO_3^{2-} on the OH groups in the brucite-like sheets through hydrogen bonds, since the number of CO_3^{2-} groups is only half that of NO_3^-. This band can thus be assigned to the δ-mode of the OH groups.[25,26]

Thermal Decomposition Processes. Figure 3 gives the TGA/DTA scans for the two as-prepared samples. In air, the $Co-NO_3$ sample undergoes two major thermal events at 145 and 177 °C, whereas the $Co-CO_3$ goes through only one major endothermic process at 142 °C and a small one at around 180 °C. In general, the first broad bands of DTA at 145 and 142 °C in both DTA scans are mainly due to the removal of various kinds of water such as interlayer water and surface adsorbed water.[18,19,27] It should be mentioned the thermal behaviors of $Co-NO_3$ in air and in nitrogen are quite similar, except for some peak shifts to higher temperatures in nitrogen (Figure 3b). On the contrary, $Co-CO_3$ shows substantial differences in the two heating atmospheres. These observations will be addressed in the final subsection.

According to the IR spectra displayed in Figure 4a, the Co_3O_4 phase has started to form at 165 °C, which is indicated in the two well-resolved IR peaks at 660 and 580 cm^{-1},[28,29] although NO_3^- still remains. In connection with this decomposition process, the IR absorption peaks at 1470 cm^{-1} (the symmetric vibration mode of monodentate nitrate), 1310 cm^{-1} (the antisymmetric vibration mode of monodentate nitrate), and 1010 cm^{-1} (activated ν_1 mode of D_{3h}) emerge, which indicates a degeneracy of D_{3h} to C_{2v} for the nitrate anions.[16,17,25−27,30,31] Although the oxidation of Co^{2+} with molecular O_2 is an exothermic reaction,[32,33] there is no such an exothermic event observed in the DTA scan of Figure 3a. This observation suggests the presence of a simultaneous or close endothermic effect. Noting that the decomposition of nitrate anions is an endothermic process,[34] a cancellation of overall thermal effects due to the involvement of nitrate anions in the oxidation can be expected. Indeed, the second thermal process (at 177 °C) takes

(15) *Powder Diffraction File*; JSPDS: Swarthmore, PA, 1995; Card No. 14-0191.
(16) Fernandez, J. M.; Barriga, C.; Ulibarri, M. A.; Labajos, F. M.; Rives, V. *J. Mater. Chem*. **1994**, *4*, 1117.
(17) Chisem, I. C.; Jones, W. *J. Mater. Chem*. **1994**, *4*, 1737.
(18) Kannan, S.; Swamy, C. S. *J. Mater. Sci. Lett.* **1992**, *11*, 1585.
(19) Grey, I. E.; Ragozzini, R. *J. Solid State Chem*. **1991**, *94*, 244.
(20) Turek, A. M.; Wachs, I. E.; Canio, E. D. *J. Phys. Chem*. **1992**, *96*, 5000.
(21) Kiselev, V. F.; Krylov, O. V. In *Adsorption and Catalysis on Transition Metals and Their Oxides*; Jehng, G., Gomer, R., Eds.; Springer-Verlag: Berlin, 1989; Vol. 9.
(22) Wachs, I. E. *Colloids Surf., A* **1995**, *105*, 1434.
(23) Labajos, F. M.; Rives, V. *Inorg. Chem*. **1996**, *35*, 5313.
(24) Busca, G.; Trifiro, F.; Vaccari, A. *Langmuir* **1990**, *6*, 1440.
(25) Ehlsissen, K. T.; Delahaye-Vidal, A.; Genin, P.; Figlarz, M.; Willmann, P. *J. Mater. Chem*. **1993**, *3*, 883.
(26) Hernandez-Moreno, M. J.; Ulibarri, M. A.; Rendon, J. L.; Serna, C. J. *Phys. Chem. Miner.* **1985**, *12*, 34.
(27) Schraml-Marth, M.; Wokaun, A.; Baiker, A. *J. Catal.* **1992**, *138*, 306.
(28) Qian, M.; Zeng, H. C. *J. Mater. Chem*. **1997**, *7*, 493.
(29) Gaddsden, J. A. *Infrared Spectra of Minerals and Related Inorganic Compounds*; Butterworth: London, 1975; p 44.
(30) Zotov, N.; Petrov, K.; Dimitrova-Pankova, M. *J. Phys. Chem. Solids* **1990**, *51*, 1199.
(31) Kruissink, E.; Reijen, L. L.; Ross, J. R. H. *J. Chem. Soc., Faraday Trans. 1* **1981**, *77*, 649.
(32) Ulibarri, M. A.; Hernandez, M. J.; Labajos, F. M.; Rives, V. *Chem. Mater.* **1991**, *3*, 626.
(33) Acro, M.; Trujillano, R.; Rives, V. *J. Mater. Chem*. **1998**, *8*, 761.

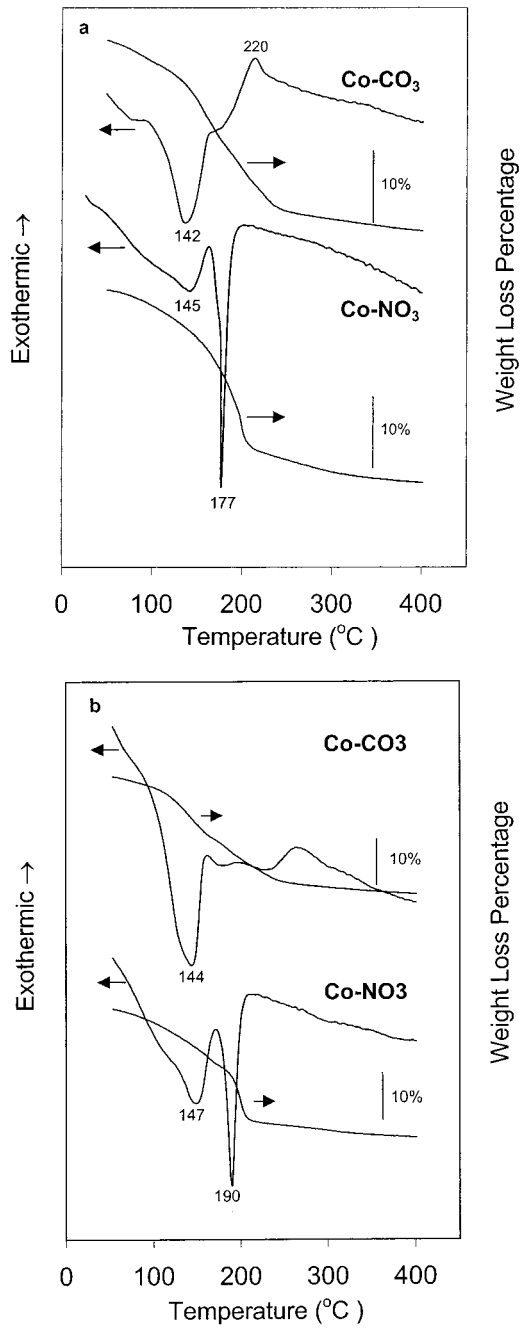

Figure 3. DTA and TGA curves of two as-prepared hydrotalcite-like precursors Co−NO_3 and Co−CO_3 in (a) air and (b) nitrogen (gas flow rate = 40 cm^3 min^{-1}).

place with a very sharp and strong endothermic peak. The decomposition of nitrate anions over this temperature range is clearly evidenced, because all of the C_{2v} modes of NO_3^- vibrations are gone leaving only a reducing peak at 1384 cm^{-1} (200 °C, Figure 4a).[16,17,25−27,30,31] On the basis of the DTA scan (Figure 3a) and the FTIR spectra (Figure 4a), it is known that the decomposition of NO_3^- (1384 cm^{-1}, D_{3h} symmetry) was continued until 400 °C, even though the oxidation formation of Co_3O_4 had been largely completed before 200 °C.

The FTIR spectrum (Figure 4b) for the 150 °C-calcined sample of Co−CO_3 shows a significant degeneracy of the D_{3h} symmetry to C_{2v} for the carbonate anions, as evidenced in stronger absorptions at 1480 and 1050 cm^{-1}.[20−23] On the basis of intensities of IR absorptions, it can be concluded that the decomposition of CO_3^{2-} and dehydroxylation have taken place over 150−200 °C. These thermal processes can be related to the endothermic shoulder at ca. 180 °C in the DTA scan (Figure 3a). However, it should be mentioned that the CO_3^{2-} with C_{2v} symmetry retains even at 250 °C in the sample of Co−CO_3 whereas the NO_3^- with C_{2v} symmetry has gone largely before 200 °C in the Co−NO_3. The remaining CO_3^{2-} (and trace NO_3^-) was decomposed continuously until 400 °C, as shown in both Figures 3a and 4b. Similar to the Co−NO_3, the Co_3O_4 phase appears at as low as 150 °C in the heated Co−CO_3 samples (Figure 4b). Note that the intensities of the two spinel bands are almost identical in all spectra but there are significant differences in their relative intensities. The full development of the pure spinel phase occurs only at temperatures >250 °C when anions/water are largely removed.

In good agreement with the above FTIR results, actually, a well-defined Co_3O_4 phase has been formed after calcination at 150 °C for 2 h, as shown in the XRD patterns in Figure 5 for both Co−NO_3 and Co−CO_3. These process assignments will be further confirmed with our in-situ TGA-FTIR study for gas-phase products in the final subsection.

Particle Sizes and Surface Areas. Although the XRD patterns of the spinel phase are extremely close and similar for both samples,[35] their derived crystallite-size data are substantially different. The effect of the calcination temperature on the crystallinity of the Co_3O_4 phase is reported in Table 2. As can been seen, the smallest crystallites obtained at 200 °C are resulted from the reactions over the second endothermic events (Figure 3). At higher calcination temperatures, the size of the crystallites increases, which can be attributed to the thermally promoted crystallite growth. The measured adsorption−desorption isotherms belong to type H-3 hysteresis.[36] The change of specific surface areas of the two hydrotalcite-like compounds upon the heat treatment is also listed in Table 2. As expected, the 200 °C-prepared samples have the highest surface areas, read as 150 and 90 m^2 g^{-1}. Apparently, the surface areas can be correlated to the crystallite sizes; i.e., smaller size crystallites give larger specific surface areas. The calculated surface area data (S_t) are also listed in Table 2, and they are in good agreement with the measured S_{BET}s, especially for the low-temperature range of 200−300 °C. At higher temperatures, however, secondary recrystallization takes place at the expense of the smaller crystallites to form large ones;[37] i.e., the point contact model is no longer held.

In general, the sample series prepared from Co−CO_3 give higher surface areas than those from Co−NO_3 (Table 2). The gaps between the measured surface areas

(34) Knacke, O.; Kubaschewski, O.; Hesselmann, K. *Thermochemical Properties of Inorganic Substances*; Springer-Verlag: Berlin, 1991; Vol. I. On the basis of the calculation from the data available from the book, the endothermic effect for $Co(NO_3)_2$ decomposition to Co_3O_4 in the air can be as high as 544.5 kJ/mol of Co_3O_4.

(35) *Powder Diffraction File*; JSPDS: Swarthmore, PA, 1995; Card No. 43-1003.

(36) Sing, K. S. W.; Everett, D. H.; Haul, R. A. W.; Moscou, L.; Pierotti, R. A.; Rouquerol, J.; Siemieniewska, T. *Pure Appl. Chem.* **1985**, *57*, 603.

(37) Zeng, H. C.; Tung, S. K. *Chem. Mater.* **1996**, *8*, 2667.

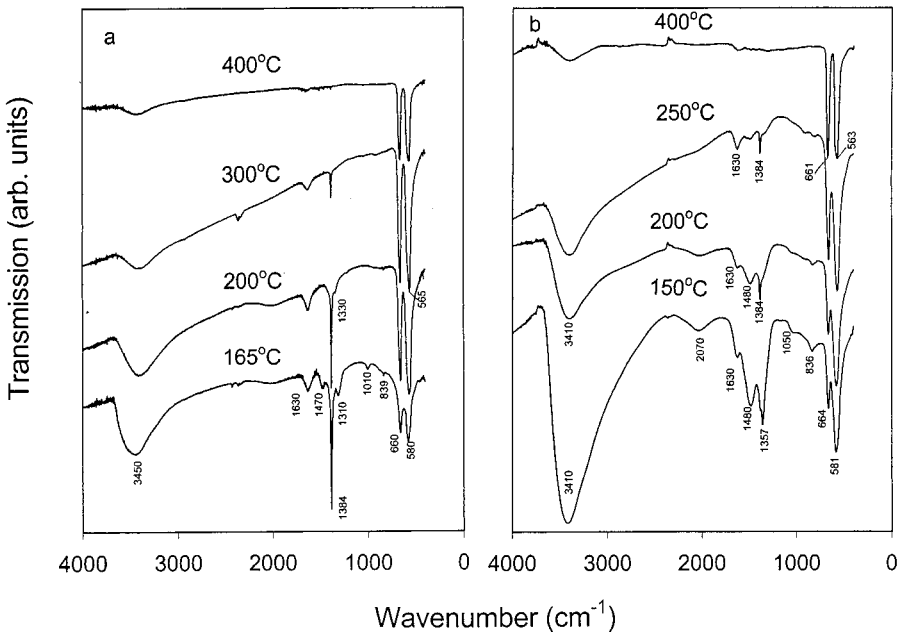

Figure 4. FTIR spectra of the heated samples: (a) Co−NO_3; (b) Co−CO_3 after heating to a specific temperature in the DTA scans.

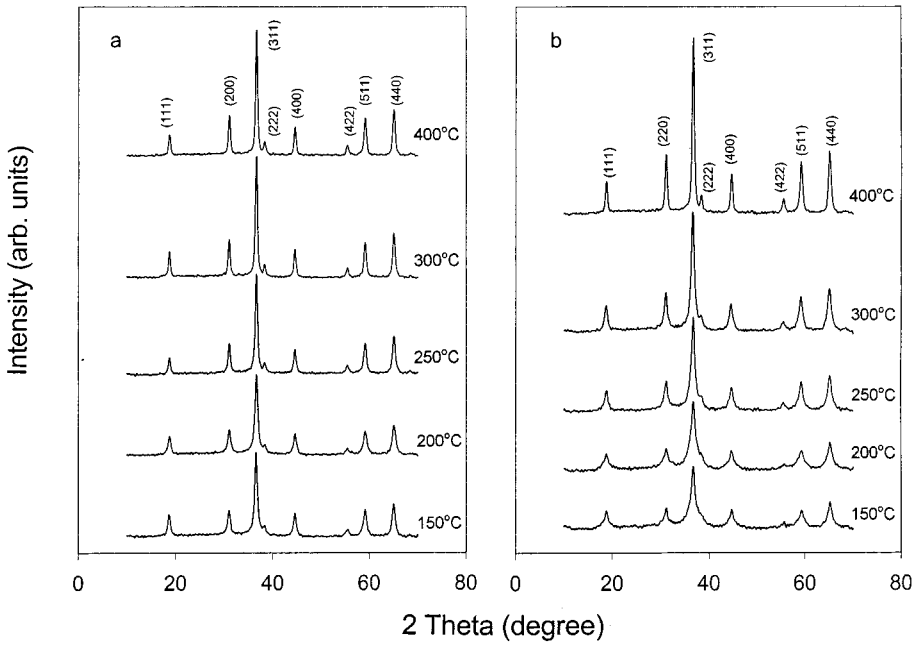

Figure 5. XRD patterns of the heated samples: (a) Co−NO_3; (b) Co−CO_3 after heated at various temperatures for 2 h.

Table 2. Data of Average Particle Size, Specific Surface Area, and Pore Volume for the Samples after Calcinations for 2 h

temp (°C)	av particle size (nm)[a]		specific surf area (m^2/g)		pore vol (cm^3/g)	
	Co−NO_3	Co−CO_3	Co−NO_3	Co−CO_3	Co−NO_3	Co−CO_3
150	13.1	8.4	67 (76)[b]	147 (119)	0.19	0.34
200	11.7	7.4	90 (86)	150 (135)	0.41	0.63
250	15.5	10.4	62 (66)	97 (96)	0.24	0.35
300	16.5	11.5	60 (61)	77 (87)	0.17	0.31
400	17.1	15.9	34 (58)	48 (63)	0.13	0.24
500	26.0	25.8	30 (38)	28 (38)	0.10	0.09
600	34.3	33.8	27 (29)	17 (29)	0.05	0.05

[a] Crystallite size is calculated from fwhms of (311) peaks of XRD patterns (Figure 5) using the Debye−Scherrer formula,[10] noting that the spinel Co_3O_4 is in cubic phase. [b] Data S_t in the parentheses are calculated from $S_t = 3/rd$, where r is the radius of crystallite size (calculated from Figure 5) and d the density of Co_3O_4 (6.06 g cm^3),[39] assuming Co_3O_4 crystallites are spherical and in point contact.

for the two series of samples are large at low-temperatures while they are closing up at higher temperatures.

Pore Volumes and Pore-Size Distributions. The change of pore volume (pore sizes summed over 2−50 nm, Table 2) follows the similar trend as the change of the surface areas. At 200 °C, the heated samples are the most porous and further heating at higher temperatures causes a significant reduction in the pore volume.

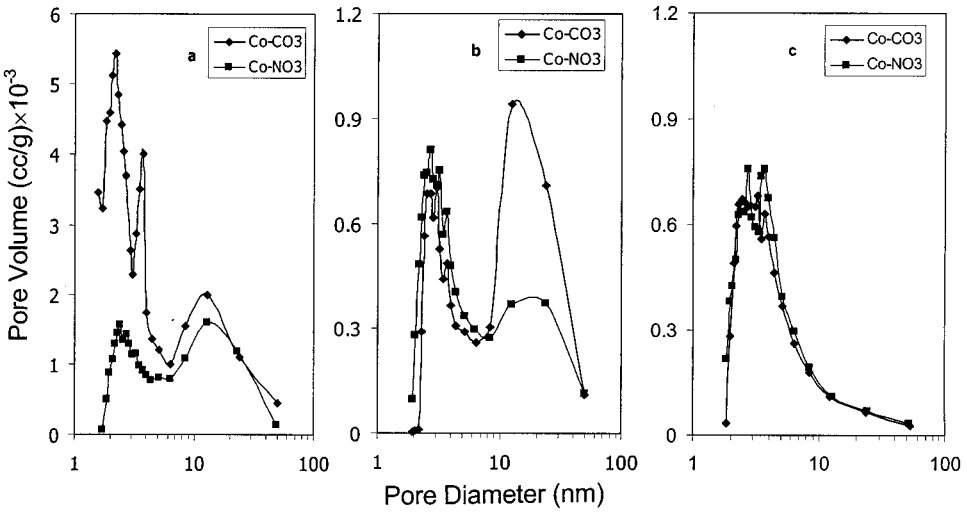

Figure 6. Pore-size distribution profiles for the heated samples: (a) after heated at 200 °C for 2 h; (b) after heated at 400 °C for 2 h; (c) after heated at 600 °C for 2 h.

Figure 6 shows the pore-size distributions for the two sample series at 200, 400, and 600 °C. The 200 °C samples (Figure 6a) generally have more mesopores than the macropores, especially the Co−CO_3 sample that shows two peaks at 2.2 and 3.7 nm. The difference between both curves for diameters below ca. 9−10 nm is marked, but they are almost coincident above 10 nm. Due to the crystallite growth at higher temperatures, the mesopores and macropores are much less after the calcination at 400 °C (Figure 6b).

The pore volume of the heated sample of Co−CO_3 is about 50−80% higher than that of the Co−NO_3 at the same studied temperatures below 500 °C (Table 2). In terms of pore-size distribution, the gain in pore volume at 200 °C is mainly due to a much higher population of small pores for Co−CO_3 (Figure 6a). On the other hand, the gain in pore volume for the same sample at 400 °C is attributed to a much larger population of macropores, noting that the pore numbers in the small diameter region are about the same in the both samples (Figure 6b). After the samples are heated at 600 °C, there are only mesopores (Figure 6c) left in the both samples and the particle sizes and pore volumes for the two samples were virtually identical (34 nm and 0.05 $cm^3\ g^{-1}$, Table 2).

Mechanisms for Spinel Oxide Formation. Concerning the decomposition of anions in Figure 3a, Co−NO_3 decomposes over a narrow temperature range (150−200 °C), while the range for the Co−CO_3 is much wider (150−250 °C). The rapid reaction and the huge heat absorbed in the Co−NO_3 sample indicate the reaction between the NO_3^- and brucite-like sheets is much more violent. Since the final decomposed products from the two samples are the same (Co_3O_4), which requires an oxidation of Co^{2+} in the octahedra, the role of the anions during the decomposition needs to be further considered. First of all, the anions may simply act as tiny "bombs" during the decomposition, noting that they turn from solid state to gaseous products from the following reactions:

$$NO_3^-\ (\text{in interlayer}) \rightarrow NO_2(g) + {}^1/_2O_2 + e^- \quad (1)$$

$$CO_3^{2-}\ (\text{in interlayer}) \rightarrow CO_2(g) + {}^1/_2O_2 + 2e^- \quad (2)$$

Since the number of NO_3^- groups is twice that of CO_3^{2-}, the gas volume produced in the Co−NO_3 should be two times of that in Co−CO_3, leading to smaller crystallite size of Co_3O_4. Nevertheless, this is not the case (Table 2), which contradicts the explosive role of the anions. Second, the oxygen atoms generated during the anion decomposition (eqs 1 and 2) may be utilized as an oxygen source for the Co_3O_4 formation. Unlike the oxygen molecules from the gas phase, which requires surface adsorption and molecular dissociation, the oxygen from the NO_3^- and CO_3^{2-} anions has been already fixed in the solid phase. As shown in Figure 4, the observed C_{2v} modes suggest a direct attachment of the anion oxygen to the central Co^{2+} cations,[16,17,20−23,25−27,30,31] leading to the decomposition of the anions and formation of cobalt oxides:

$$Co^{2+} + O^- - NO_2 = Co^{2+}O^- - NO_2 \quad (3.1)$$

$$Co^{2+}O^- - NO_2 = Co^{3+}O^{2-} + NO_2(g) \quad (3.2)$$

$$Co^{2+} + O^{2-} - CO_2 = Co^{2+}O^{2-} - CO_2 \quad (4.1)$$

$$Co^{2+} + O^{2-} - CO_2 = Co^{2+}O^{2-} + CO_2(g) \quad (4.2)$$

The formation of Co_3O_4 requires 2/3 of cobalt to be in the trivalent state. This oxidation might be pursued directly in the NO_3^- case that involves a redox reaction eq 3.2, noting the fact that the decomposition of the Co−NO_3 sample is not too dependent on the TGA/DTA atmosphere employed (Figure 3). In principle, the oxidation of Co^{2+} by utilizing the solid matrix oxidant NO_3^- should be more advantageous in the formation of Co_3O_4 than using the gaseous oxygen, as eq 3.2 is a diffusionless process. Figure 7 shows a schematic drawing for our proposed redox mechanism, which is analogous to a so-called "grafting process" for decomposition of oxometalates.[38] The mechanism is further supported by our in-situ TGA-FTIR investigation on the decomposed gas products. As reported in Figure 8a, when NO_3^- anions are the major species in the gallery space, the dehydroxylation, decomposition of CO_3^{2-} and NO_3^-, and oxidation of divalent cobalt take place at the same temperature (ca. 184−190 °C), which seems to explain

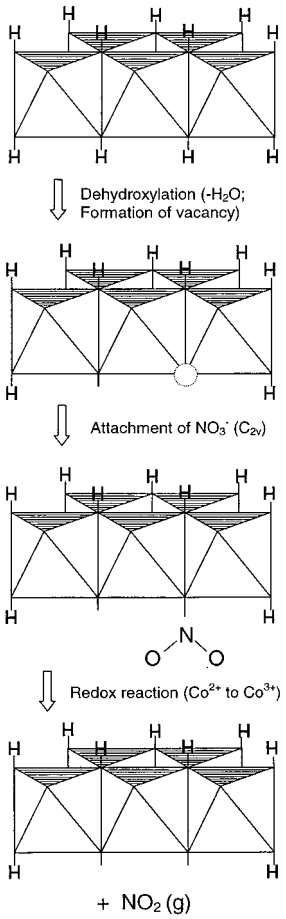

Figure 7. Proposed mechanism for the direct redox reaction between the oxidative anion NO_3^- and Co^{2+} during the decomposition of $Co-NO_3$. Oxygen atoms (not shown) are located at the corners of octahedrons in the brucite-like sheets.

why there is no exothermic effect in the DTA curve of the $Co-NO_3$ sample (Figure 3). The sharp NO_2 peak (190 °C) can be related to the chemical reactions of eqs 3.1 and 3.2 (see Figure 4a: NO_3^- in C_{2v}, 165−200 °C), while the broad shoulder (ca. 255 °C) can be assigned to the decomposition of nitrate anions which are not directly attached to cobalt cations (see Figure 4a: NO_3^- in D_{3h}, 200−300 °C). On the contrary, dehydroxylation and decomposition of carbonate are separated to some extent when CO_3^{2-} anions are predominant (Figure 8b). In particular, the formation of CO_2 is peaked at 205 °C while the oxidation of divalent cobalt continues to a higher temperature, noting that a small exothermic peak is still can be seen at 220 °C in Figure 3a. At higher temperatures, the dissociation of the gaseous oxygen and oxygen diffusion are no longer a problem, which irons out the differences between NO_3^- and CO_3^{2-} in the Co_3O_4 formation. As reported earlier, pore sizes and pore volumes for the 600 °C-heated hydrotalcite-like precursors are virtually identical (Table 2), since the oxidative formation of Co_3O_4 becomes thermodynamically controlled at high temperatures.

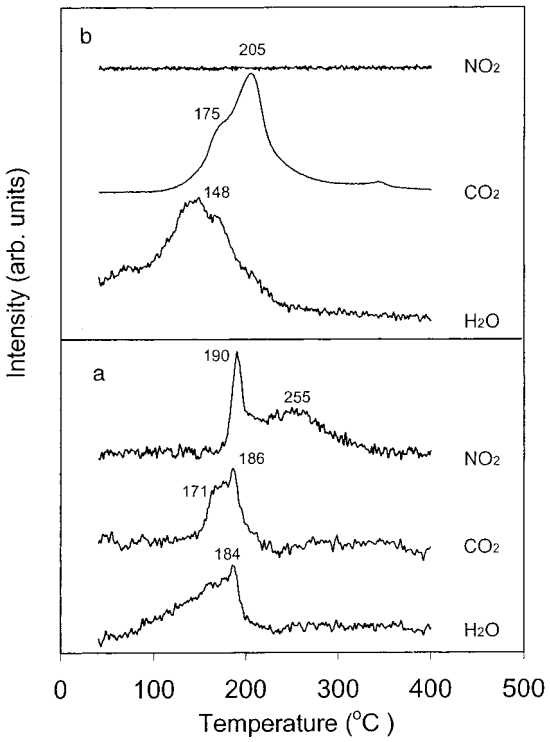

Figure 8. Integrated absorbance of evolved gases H_2O, CO_2, and NO_2 versus temperature in the combined TGA−FTIR measurements for the samples of (a) $Co-NO_3$ and (b) $Co-CO_3$ (air flow rate = 100 cm^3 min^{-1}).

Conclusions

In summary, the crystallite size, surface area, and pore structure of the spinel Co_3O_4 can be manipulated by intercalation of oxidative or nonoxidative anions in the $Co^{II,III}$-hydrotalcite-like compounds. It is found that the Co_3O_4 crystallites derived from the CO_3^{2-}-intercalating hydrotalcite-like precursor are systematically smaller than those from the NO_3^--intercalating compound at the same decomposition temperatures of 150−600 °C. The surface area of the prepared Co_3O_4 can be correlated to the crystallite size by a simple ball-like model. The pore volume gains using the CO_3^{2-}-intercalating hydrotalcite-like precursor are due to increases in the population of mesopores or macropores. By selection of the nonoxidative anions, the Co_3O_4 spinel with crystallite size of 7−34 nm and surface area of 17−150 m^2/g can be prepared at 150−600 °C. In particular, nanometer size Co_3O_4 crystallites (7−10 nm) can be synthesized at 150−250 °C from the CO_3^{2-}-intercalating hydrotalcite-like precursor. The differences observed in the final Co_3O_4 spinel can be attributed to chemical reactivity of the intercalated anions, especially the oxidative ability of the anions with the metal cations in the brucite-like sheets.

Acknowledgment. The authors gratefully acknowledge research funding (Grants RP3999902/A and A/C50384) cosupported by the Ministry of Education and the National Science and Technology Board of Singapore.

CM000371E

(38) (a) Malherbe, F.; Bigey, L.; Forano, C.; deRoy, A.; Besse, J. P. *J. Chem. Soc., Dalton Trans.* **1999**, *21*, 3831. (b) Depege, C.; ElMetoui, F. Z.; Forano, C.; deRoy, A.; Dupuis, J.; Besse, J. P. *Chem. Mater.* **1996**, *8*, 952. (c) Depege, C.; Bigey, L.; Forano, C.; deRoy, A.; Besse, J. P. *J. Solid State Chem.* **1996**, *126*, 314.

(39) Sakamoto, S.; Yoshonaka, M.; Hirota, K.; Yamaguchi, O. *J. Am. Ceram. Soc.* **1997**, *80*, 267.